Received 5 May 2021; revised 7 June 2021; accepted 9 June 2021. Date of publication 14 June 2021; date of current version 18 June 2021.

Digital Object Identifier 10.1109/OJAP.2021.3089046

Antenna Aperture Synthesis Using Mode-Converting Metasurfaces

FARIS ALSOLAMY (Member, IEEE), AND ANTHONY GRBIC (Fellow, IEEE)

Electrical Engineering and Computer Science Department, University of Michigan at Ann Arbor, Ann Arbor, MI 48109, USA

CORRESPONDING AUTHOR: A. GRBIC (e-mail: agrbic@umich.edu)

This work was supported by the UM-KACST Joint Center for Microwave Sensor Technology.

ABSTRACT Mode-converting metasurfaces are passive, lossless devices that can be designed to transform a set of incident modes to a desired set of transmitted modes. In this paper, mode-converting metasurfaces are utilized to synthesize arbitrary, azimuthally-invariant TM apertures. The methods presented in this work can be used to design antennas that can meet specific near-field and far-field criteria unlike most metasurfaces which solely manipulate the far field. The proposed antennas consist of a coaxially-excited, radial cavity topped by the mode-converting metasurface. The main role of the mode-converting metasurface is to establish the desired aperture by converting the modal distribution of the excitation to that of desired aperture. Its secondary role is to impedance match the coaxial feed to the radial cavity. Using modal network theory, an optimization-based design procedure is developed to synthesize the proposed metasurface antennas. The admittance profiles of the electric sheets that comprise the metasurface are optimized to establish the desired aperture profile. To illustrate the design procedure, a radial Gaussian beam antenna is synthesized at 10 GHz and its performance is verified using a full wave electromagnetic solver. The proposed antenna has a height and weight advantage over Gaussian beam horn antennas.

INDEX TERMS Metasurface antennas, aperture synthesis, modal network theory, mode conversion, radial Gaussian beam.

I. INTRODUCTION

DUE TO their negligible thickness compared to the wavelength, metasurfaces have enabled the design of numerous low-profile microwave and optical devices [1], [2]. At microwave and millimeter wave frequencies, metasurfaces are often realized as printed metallic claddings on thin dielectric substrates. Metasurfaces are modeled theoretically as either a single infinitesimally-thin bianisotropic sheet using generalized sheet transition conditions (GSTCs) or as a stack of infinitesimally-thin, electric sheets separated by dielectric spacers [3]–[6]. GSTCs relate the magnetic and electric surface currents on a sheet to the average fields at a sheet [7], [8].

Both models are used to design metasurface-based devices for a variety of applications. These applications include, antenna design [9], control of guided modes [3], [10], polarization conversion [5], [6], and wavefront manipulation [11]. Nonetheless, as explained in [3], the cascaded electric sheet model is indeed better than the GSTC model for two main reasons. First, the cascaded sheet model takes into account the finite thickness of the metasurface and therefore models spatial dispersion. Second, a lossless and passive GSTC has to conserve power locally through its surface. Thus, it cannot be used to reshape the normal power density profile, without introducing reflection or additional auxiliary surface waves onto its outer surfaces [12]. On the other hand, a lossless, passive cascaded-sheet metasurface can be synthesized to reshape the normal power density profile without these requirements [3].

In general, metasurface-based antennas, or simply metasurface antennas, can be designed to have desired aperture profiles or radiation patterns [13], [14]. This can be achieved by tailoring the metasurface's individual cells. Metasurface antennas can serve as a low-profile, simple-to-feed alternative to conventional antenna arrays, reflectors, or reflectarrays. They are typically designed using a single electric sheet above a grounded dielectric substrate. This design approach is simple and yields practically realizable antennas. Typically,

the electric sheet of these metasurface antennas is realized as a printed metallic cladding. Examples of this class of antennas include modulated metasurface antennas [14], [15], and reflectarray antennas [16]. Nonetheless, a single electric sheet does not provide sufficient degrees of freedom to control both the magnitude and the phase of the aperture field. In order to increase the degrees of freedom, a weakly radiative (WR) field [14] or surface waves [16] should be incorporated into the desired aperture field. Introducing WR fields or surface waves to the desired aperture profile, distorts the near field of the antenna. Therefore, a single electric sheet antenna cannot be designed to meet specific near field criteria.

Another approach to attain added degrees of freedom is to use a bianisotropic sheet in lieu of the electric sheet. In general, a reciprocal, bianisotropic sheet is described using three non-vanishing tensors [4], [6]. Following the notation in [6], these three 2×2 or 3×3 tensors are: the electric admittance $\overline{\overline{\mathrm{Y}}}$, the magnetic impedance $\overline{\overline{\mathrm{Z}}}$, and the magnetoelectric coupling coefficient $\overline{\overline{\mathrm{X}}}$. These tensors define the GSTC. GSTCs are local boundary conditions that relate the electric and the magnetic surface currents on the sheet to the average fields at the sheet. As noted earlier, the normal power density profile must be continuous across a bianisotropic sheet. Such a constraint, in fact, limits metasurface functionality. For instance, a lossless, passive, and reflectionless bianisotropic sheet cannot be synthesized to reshape the incident normal power profile, unless auxiliary surface waves are added to the solution. Adding auxiliary surface waves, does not affect an antenna's far field but does alter its near field. Additionally, bianisotropic sheets are challenging to realize in practice. A three-sheet implementation [4], [6] of the idealized bianisotropic boundaries requires extremely thin dielectric spacers [12]. In addition, the spatial dispersion resulting from the finite thickness of the three-sheet cascade, and the transverse propagation of the fields between the three sheets are neglected in the design procedure. All these factors deteriorate the realized metasurface performance.

In this paper, we propose a framework to design a metasurface antenna consisting of cascaded sheets, as shown in Fig. 1. The cascaded sheet metasurface is composed of tightly-coupled, electric sheets that are separated by dielectric spacers. The mainstay of the proposed antenna is the cascaded sheet metasurface that acts as a mode converter. The mode-converting metasurface is a passive, and lossless device that can be designed to transform a set of incident modes to a set of desired transmitted modes, as shown in Fig. 1. Since the metasurface comprises multiple sheets, added degrees of freedom are available to control the far field without relinquishing control over the near field. As a result, the proposed antenna can be designed to meet specific far-field and near-field criteria. In addition, the finite thickness of the metasurface is accounted for throughout the design procedure. Thus, spatial dispersion is accounted for, and the fields within the metasurface

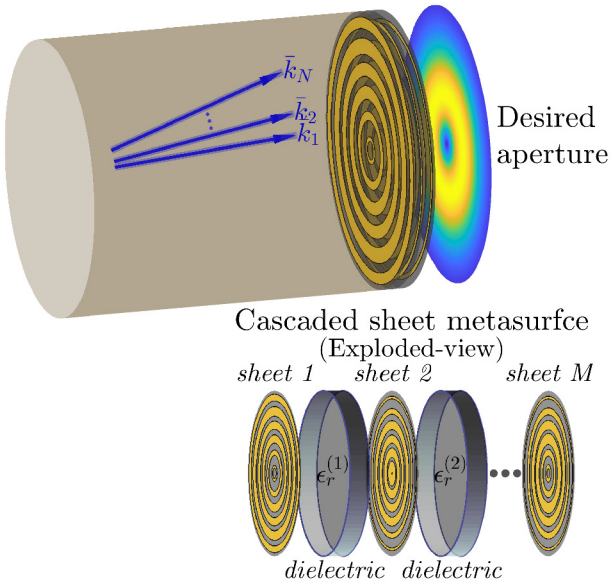

FIGURE 1. A cascaded sheet mode-converting metasurface used to synthesize, in both amplitude and phase, a desired azimuthally invariant aperture profile. The mode-converting consists of multiple electric sheets separated by dielectric spacers.

are accurately modeled. The proposed design framework is shown for azimuthally-invariant apertures. Such apertures can support cylindrical vector beams, which include: Bessel beams, radial Gaussian beams, and higher-order Gaussian beams (Laguerre-Gaussian beams) [17], [18]. Moreover, cylindrical vector beams include azimuthally variant beams such as vortices or orbital angular momentum apertures, which could be excited by azimuthally variant apertures. Cylindrical vector beams incur minimal diffraction as they propagate within the Fresnel zone. Therefore, they can be used in the design of wireless power transfer systems within the radiative near field [17]. In this paper, we consider cylindrical TM_{0n} modes and therefore TM, azimuthally invariant apertures. These modes can be easily generated by a radial cavity covered by a mode-converting metasurface using a central coaxial feed. The analysis presented here can be easily modified for cylindrical TE apertures.

II. BUILDING BLOCKS OF THE ANTENNA

As depicted in Fig. 2, central to the proposed antenna is a radial cavity. To ensure azimuthally-invariant, TM aperture fields, the cavity is coaxially-fed at its center and topped by an azimuthally invariant cascaded sheet, mode-converting metasurface. The mode-converting metasurface establishes the desired aperture by converting the modal distribution of the coaxial feed to the modal distribution of the desired aperture. In theory, the modal distribution of the desired aperture can include as many evanescent modes as needed. As shown in Fig. 2, the antenna can be viewed as the integration of three main building blocks. The antenna's building blocks are: the radial cavity, the mode-converting metasurface, and the coaxial-to-waveguide junction.

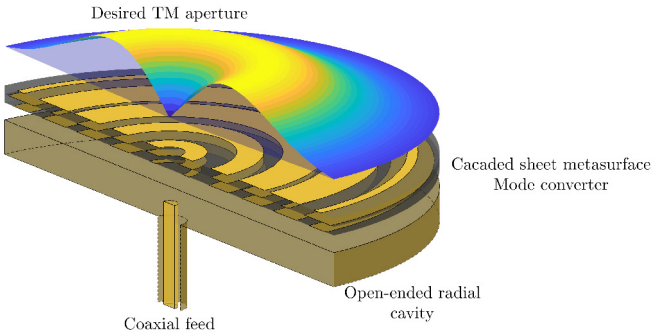

FIGURE 2. A low-profile metasurface-based antenna that can be designed to generate an arbitrary azimuthally invariant TM aperture profile. The antenna consists of a coaxially-fed radial cavity topped by a cascaded-sheet, mode-converting metasurface.

Modal network theory, which was originally developed to characterize waveguide discontinuities [19], is ideally suited to analyze and design such antennas consisting of cascaded electric sheets in a waveguide. The ports of the modal network represent the modal voltages and the modal currents of the waveguide's eigenmodes [20]. This is, in contrast to the well-known microwave network theory, where ports of the microwave circuit network represent voltages and currents at the circuit terminals [21]. Hence, the distinct name modal network theory. In modal network theory, as in microwave network theory, the modal network parameters of each building block can be calculated separately. Subsequently, these modal network parameters can be cascaded/combined using standard matrix operations. Modal network parameters relate the modal coefficients of the waveguide eigenmodes to each other at the input and at the output of a given block [3]. Typically, modal network parameters are given in matrix form. Examples of modal matrices include the modal scattering matrix, the modal impedance matrix, and the modal wave matrix. Throughout this paper, the modal scattering matrix will be utilized most often. The modal scattering matrix relates the incident and the reflected modes on both sides of a waveguide section. Further details concerning the modal network theory implementation and its usefulness will be presented in the following subsections, as the context requires.

In the following subsections, we will briefly discuss each building block of the antenna. Specifically, we will show how the modal scattering matrix of each building block can be calculated. First, the radial cavity will be considered, then the mode-converting metasurface, and finally the coaxial-to-waveguide junction.

A. RADIAL CAVITY

In recent years, radial cavities have been used as a base for multiple low-profile, simple-to-fabricate, metasurface antennas. For example, radial Bessel beam launchers that are composed of an air-filled or dielectric-filled radial cavity topped by a capacitive electric sheet, were reported in [22]–[24]. Other examples include linearly and circularly polarized antennas fed by a Bessel beam reported in [25].

Fields inside a cavity propagate/evanesce as a finite set of orthogonal, discrete modes (modal spectrum). The spatial frequencies of these discrete modes are dictated by the radius and the materials of the cavity. In the free space region, outside the cavity, the fields have a continuous spatial spectrum. Analyzing an open-ended radial cavity, or in general any open-ended cavity, involves matching the tangential components of the discrete modes of the cavity to the tangential free-space fields at the cavity aperture. Again, in this work the focus will be on cylindrical TM_{0n} modes and TM apertures fields. In [26], the simple case of a radial waveguide supporting only the TM_{01} was considered in detail. The general case of an open-ended radial waveguide supporting an arbitrary superposition of TM_{0n} modes was treated in [27].

Here, we will follow a slightly different approach than the one reported in [27]. The tangential electric field of the aperture will be expanded into a Fourier-Bessel series that is identical to the modal expansion of the waveguide fields. Such an expansion is justified by the fact that over the aperture's plane, the tangential electric field vanishes everywhere outside the aperture. The aperture's tangential electric field uniquely and completely defines the fields everywhere in the free space region above the cavity.

To begin, let's recall the modal expansion of the azimuthally invariant TM fields inside a cylindrical waveguide,

$$E_\rho = \sum_{n=1}^{\infty} \frac{\sqrt{\eta_n}}{u_n}\left(a_n e^{-ik_{zn}z} + b_n e^{ik_{zn}z}\right) J_1\left(\frac{j_n}{R}\rho\right) \tag{1}$$

$$H_\phi = \sum_{n=1}^{\infty} \frac{1}{u_n\sqrt{\eta_n}}\left(a_n e^{-ik_{zn}z} - b_n e^{ik_{zn}z}\right) J_1\left(\frac{j_n}{R}\rho\right), \tag{2}$$

where, j_n is the *nth* null of $J_0(.)$ and $J_0'(.) = -J_1(.)$. R is the waveguide radius. For the *nth* mode, a_n and b_n denote the forward and backward modal coefficients, respectively, η_n, and k_{zn} denote the TM modal wave impedance, and the propagation constant, respectively. The TM modal wave impedance η_n, and the propagation constant k_{zn} take the form,

$$\eta_n = \frac{k_{zn}}{\omega\epsilon_0\epsilon_r} \tag{3}$$

$$k_{zn} = \begin{cases} \sqrt{\omega^2\mu_0\epsilon_0\epsilon_r - \left(\frac{j_n}{R}\right)^2} & \text{for propagating modes} \\ -i\sqrt{\left(\frac{j_n}{R}\right)^2 - \omega^2\mu_0\epsilon_0\epsilon_r} & \text{for evanescent modes.} \end{cases} \tag{4}$$

The normalization factor u_n is needed to ensure that the basis functions in the modal expansions (1) and (2), have equal power. It is given by,

$$u_n = \sqrt{\frac{J_1^2(j_n)R^2}{2}}. \tag{5}$$

For simplicity, let's place the aperture at the plane $z = 0$, so the modal expansion in (1), and (2) at the aperture plane can be written as,

$$E_{\rho}^{z=0^-} = \sum_{n=1}^{N} \frac{\sqrt{\eta_n}}{u_n}(a_n + b_n)\ J_1\left(\frac{j_n}{R}\rho\right) \tag{6}$$

$$H_{\phi}^{z=0^-} = \sum_{n=1}^{N} \frac{1}{u_n\sqrt{\eta_n}}(a_n - b_n)\ J_1\left(\frac{j_n}{R}\rho\right), \tag{7}$$

where, the superscript $z = 0^-$ indicates a plane just below the aperture toward the waveguide. Note in (6), and (7), only N modes are retained in the modal expansion. Based on the arguments presented earlier, the aperture fields, from the free space side, can be expanded as a Fourier-Bessel series,

$$E_{\rho}^{z=0^+} = \sum_{n=1}^{N} \frac{e_n}{u_n}\ J_1\left(\frac{j_n}{R}\rho\right) \tag{8}$$

$$H_{\phi}^{z=0^+} = \sum_{n=1}^{N} \frac{h_n}{u_n}\ J_1\left(\frac{j_n}{R}\rho\right), \tag{9}$$

where, the superscript $z = 0^+$ indicates a plane just above the aperture toward free space.

The electric and magnetic fields in free space, as well as at the aperture plane, are related by the free space Green's function. Using the spectral form of the free space Green's function, the magnetic field coefficients h_n in (9) can be related to the electric field coefficients e_n in (8) via the spectral admittance matrix $\overline{\overline{B}}$ (provided in the Appendix). By matching the fields at the aperture plane ($z = 0$), and expressing the magnetic field coefficients h_n in terms of the electric field coefficients e_n using $\overline{\overline{B}}$, we can explicitly solve for the aperture modal reflection matrix $\overline{\overline{S}}_{Aper}$. The aperture modal reflection matrix $\overline{\overline{S}}_{Aper}$ relates the reflected modes at the open-ended cavity aperture to the incident modes as follows,

$$[b_1, b_2 \ldots, b_N]^T = \overline{\overline{S}}_{Aper}\ [a_1, a_2 \ldots, a_N]^T, \tag{10}$$

where, $\overline{\overline{S}}_{Aper}(q, p)$ is the reflection coefficient from mode p into mode q.

It is clear from (6), and (7), that the aperture fields due to any arbitrary set of incident modes can be established once $\overline{\overline{S}}_{Aper}$ is known. Specifically, the aperture electric field coefficient e_n is related to the incident mode a_n through the following relation,

$$\overline{E} = g\left(I + \overline{\overline{S}}_{Aper}\right)\overline{A}, \tag{11}$$

where, $\overline{E} = [e_1, e_2 \ldots, e_N]^T$, $\overline{A} = [a_1, a_2 \ldots, a_N]^T$, I is the $N \times N$ identity matrix, and g is a diagonal matrix defined as follows,

$$g = \begin{bmatrix} \sqrt{\eta_1} & \cdots & 0 \\ \vdots & \ddots & \vdots \\ 0 & \cdots & \sqrt{\eta_N} \end{bmatrix}. \tag{12}$$

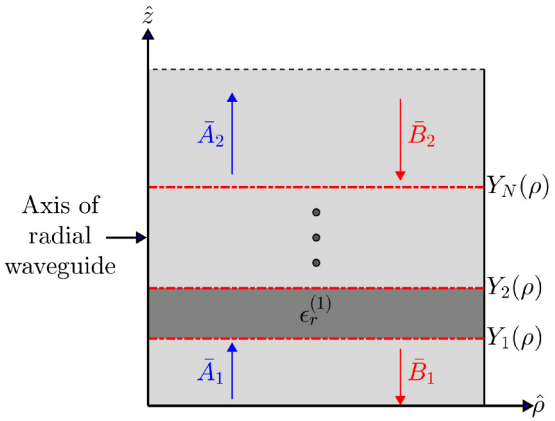

FIGURE 3. 2D side view of the cascaded-sheet, metasurface-based mode converter. It is composed of multiple electric sheets placed transversely to the $\hat{z}$ axis, and separated by dielectric spacers. Each electric sheet is described by a radially-varying electric admittance profile $Y(\rho)$. $\overline{A}$, and $\overline{B}$ denote the set of forward and backward modes, respectively, on both sides of the metasurface.

Explicit formulas and detailed deviations of the aperture's modal reflection matrix $\overline{\overline{S}}_{Aper}$, and the spectral admittance matrix $\overline{\overline{B}}$ are presented in the Appendix.

B. MODE-CONVERTING METASURFACES

Mode-converting metasurfaces are passive lossless devices, that transform a set of incident modes on both sides of the metasurface to a set of desired reflected modes on both sides of the metasurface. They consist of a stack of closely-spaced electric sheets separated by dielectric spacers, as shown in Fig. 3. The close spacing between the sheets gives rise to evanescent/higher-order coupling between the sheets. This evanescent mode interaction allows the normal power to be efficiently redistributed along the transverse direction of the metasurface [3]. Again, we are interested in azimuthally invariant TM fields, therefore the discussion here will be limited to the cylindrical TM_{0n} modes. However, the work can be generalized to both polarizations.

In earlier work, an analytical design method was proposed for synthesizing the constitutive electric sheets of a mode-converting metasurface [28]. This analytical method was limited to the simple scenario of single mode-to-single mode conversion. Later, the analytical design method [28] was replaced by an optimization-based one [3], [29]. In the optimization method, the constitutive electric sheets of the metasurface are optimized to realize targeted entries of the metasurface modal scattering matrix. This allowed the transmission of a targeted modal distribution given an arbitrary incident modal distribution. The optimization-based design method is general and is not limited to specific mode conversions. In addition, the optimization can be tailored to ensure metasurface realizability. For example, the admittance profiles of the synthesized electric sheets can be restricted to have capacitive values. As it has been shown in [3], a capacitive electric sheet can be easily realized with printed metallic rings on both sides of a thin substrate.

The analytical and the optimization-based design methods rest upon two key concepts: the Discrete Hankel Transform (DHT), and modal network theory. The DHT is an approximate, yet accurate mathematical tool that transforms fields from the spatial to the modal domain, and vise versa, using only matrix multiplication. On the other hand, modal network theory allows translation of the modes from one sheet to another also via matrix multiplication. Together, the DHT and modal network theory are ideally suited to rapidly optimize the admittance profiles of the constitutive electric sheets of the metasurface [30]. Next, the implementation and the usefulness of these two tools, the DHT and the modal network theory, will be discussed.

Field solutions within a waveguide are usually constructed in the modal (spectral) domain. Conversely, the metasurface's boundary conditions are typically stipulated in the spatial domain. As a result, the metasurface boundary conditions need to be transformed from the spatial domain to the modal domain. This transformation involves the calculation of the modal, mutual admittances between all the modes at each electric sheet of the metasurface. The exact formulas of the modal mutual admittances of an electric sheet were derived in [3]. These exact formulas require the evaluation of oscillatory integrals: the Hankel transform. In general, the Hankel transform is performed through numerical integration. Doing so, can be computationally expensive, especially if the admittance profiles of the sheets need to be optimized. Alternatively, the Hankel transform can be performed using the DHT. The DHT utilizes matrix multiplication and only specific discrete points in space to calculate the modal mutual admittances of an electric sheet. Replacing the numerical integration with simple matrix operations greatly increases the efficiency of the optimization routine. As shown in [3], the modal wave matrix of a radially inhomogeneous electric sheet can be obtained in closed-form using the DHT without the evaluation of integrals. Details concerning the DHT, its accuracy, implementation, and applications can be found in [3], [31], [32].

Another key method to the analysis and design of mode-converting metasurfaces, is modal network theory. Recently, modal network theory was extended beyond conventional geometrical waveguide discontinuities. It was applied to discontinuities caused by metasurfaces placed transversely to a waveguide axis [3]. Using modal network theory, a waveguide discontinuity can be described with a multi-port modal network. This multi-port modal network relates the waveguide's modes on both sides of the discontinuity. The mode-converting metasurface, or any of its constitutive electric sheets, can be regarded as a waveguide discontinuity. Ports of the multi-port modal network correspond to the waveguide modes on both sides of the metasurface. The characteristic impedance of each port is equal to the modal wave impedance [19].

Waveguide modes can be classified as either accessible or inaccessible (localized) modes [33]. By definition, accessible modes are those that can be detected at adjacent discontinuities. They include propagating modes, as well as evanescent modes that reach adjacent discontinuities. In contrast, inaccessible modes are only detectable very close to the discontinuity and do not interact with adjacent discontinuities. In most practical cases, a terminal description of a discontinuity is more desirable than a complete field description. Within modal network theory, a terminal description of a discontinuity is obtained by considering the ports that only pertain to accessible modes. While the ports that pertain to inaccessible modes are terminated in their reactive modal wave impedances [19], [33]. The classification of waveguide modes into accessible and inaccessible modes is more general than the well-known classification into propagating and evanescent modes [3]. Since an evanescent mode could be an accessible mode if the separation between the adjacent discontinuities (separation between the electric sheets of metasurface) is comparable to the decay length of the evanescent mode.

Different modal matrices can be used to describe modal networks. In this work, we will be using the modal scattering matrix $\overline{\overline{S}}$. The modal scattering matrix $\overline{\overline{S}}$ relates the incident modes to the reflected modes at the metasurface. For a cascaded sheet metasurface, a general method to calculate the modal scattering matrix $\overline{\overline{S}}$, as well as other modal matrices, has been derived in [3], [28]. To calculate $\overline{\overline{S}}$, first we calculate the modal wave matrix $\overline{\overline{M}}$ of each constitutive electric sheet and each dielectric spacer. It should be noted that, for an electric sheet and for a dielectric spacer the matrix $\overline{\overline{M}}$ is known in closed-form. Closed-form expressions were obtained through the use of the DHT. The modal wave matrix $\overline{\overline{M}}$ of the overall metasurface is then found by multiplying the modal wave matrices $\overline{\overline{M}}$ of the constitutive electric sheets and the dielectric spacers. Finally, the modal wave matrix of the metasurface $\overline{\overline{M}}$ is transformed to the modal scattering matrix [5]. The size of the modal scattering matrix $\overline{\overline{S}}$ is $2N \times 2N$, where N is the number of accessible modes considered in the solution.

C. COAXIAL-TO-WAVEGUIDE JUNCTION

A coaxial-to-waveguide junction is a special type of waveguide junction, where one side of the junction is attached to a coaxial line. Waveguide junctions can be analyzed via the mode matching technique (MMT). In the MMT, the fields, in the regions adjacent to the junction, are expanded as finite sums of orthogonal modes with unknown complex coefficients [34]. These unknown complex coefficients can be found by applying appropriate testing modes to enforce the continuity of the fields at the junction plane [19], [27], [35]. A detailed discussion on the implementation of the MMT can be found in [35].

In coaxial-to-waveguide junctions, the diameter of the coaxial line is typically very small compared to the wavelength. Thus only the fundamental TEM mode is assumed inside the line [27]. In the waveguide section, multiple modes

are considered in the field expansion, even if the waveguide only supports a single mode. Generally, the waveguide radius is significantly larger than the coaxial line radius. Such a large discrepancy in the radius introduces a significant impedance mismatch and causes undesired reflection. Thus, a matching network is typically needed at the junction to reduce reflection to acceptable levels. For example, in [23], a two-section matching network was implemented to match a coaxial line to an over-moded radial cavity. In the proposed metasurface antenna, no external matching network is needed. The mode-converting metasurface is designed to impedance match the coaxial line to the cavity. This is achieved by ensuring that the total radiated power of the desired aperture is equal to the incident power.

The problem considered here is a junction between a coaxial line and an over-moded radial cavity. The coaxial line is assumed to be placed at the center of the radial cavity. Due to the rotational symmetry, and the polarization of the fields in the coaxial line, only TM_{on} modes are excited in the radial cavity. This problem has been considered in detail using the MMT in [27]. In this paper, for convenience, the commercially available 3D full wave solver ANSYS HFSS is used to compute the modal scattering matrix of the coaxial-to-waveguide junction. Note, this approach will not compromise the efficiency of the optimization routine, since neither the coaxial radius nor the waveguide radius are variables in the optimization routine.

Thus far, the modal scattering matrices of the individual building blocks of the antenna have been discussed in detail. These modal scattering matrices relate the incident modes to the reflected modes at each building block of the antenna. In the coming section, we will see how these modal scattering matrices can be cascaded to compute the antenna's aperture and radiation. The synthesis of the antenna apertures through optimization will also be discussed.

III. APERTURE SYNTHESIS USING A MODE-CONVERTING METASURFACE

As noted earlier, the mode-converting metasurface is the mainstay of the proposed metasurface antenna. Thus, the design of the antenna amounts to designing of the mode-converting metasurface. The mode-converting metasurface plays two fundamental roles in the proposed metasurface antenna. First, it establishes the desired aperture profile, by converting the incident modal distribution to the modal distribution of the desired aperture. Second, it matches the coaxial feed to the radial cavity by enforcing that the total radiated power is equal to the incident power.

In the design of the proposed antenna, an optimization-based design procedure is used to synthesize the mode-converting metasurface. In this procedure, the admittance profiles of the metasurface's constitutive electric sheets are optimized to realize targeted field transformation needed to establish the aperture field. This targeted transformation is simply the transmission term of the modal scattering matrix

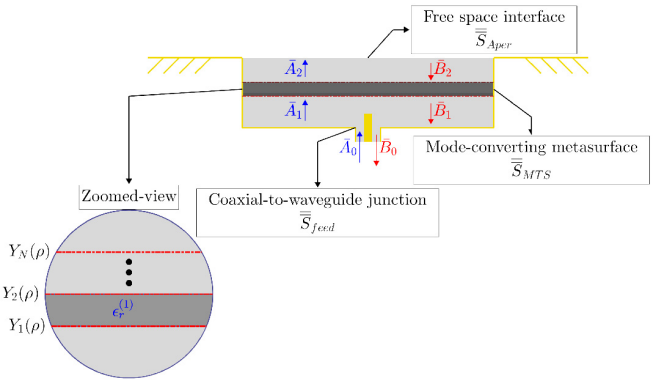

FIGURE 4. Side view of the proposed metasurface-based antenna. The antenna is divided into three main building blocks. Each building block is described by a modal scattering matrix. The modal scattering matrix relates the incident modes to the reflected modes on both sides of a given section.

applied to the incident modes. The design procedure is similar to the one reported in [3], [29]. However, in [3], [29] the mode-converting metasurface was assumed to be isolated in an infinitely-long waveguide. Therefore, the objective function of the optimization was only written in terms of the modal scattering matrix of the metasurface. Moreover, only the propagating modes were considered in the modal scattering matrix of the overall metasurface (the sheets and the spacers). In the case of the antenna design, it is clear that this assumption (isolated metasurface in an infinitely-long circular waveguide) cannot be made. Thus, the objective function should take into account the interaction between the metasurface, the coaxial feed, and the free-space interface. Further, since the antenna elements are closely spaced, higher evanescent modes should be considered in the modal scattering matrix of the mode-converting metasurface.

To solve for the radiated fields of the antenna, the modal scattering matrices of the individual building blocks of the antenna are cascaded. As shown in Fig. 4, the modal scattering matrices of the individual building blocks are labeled as follows, $\overline{\overline{S}}_{feed}$ represents the modal scattering matrix of the coax-to-waveguide junction, $\overline{\overline{S}}_{MTS}$ represents the modal scattering matrix of the mode-converting metasurface, and $\overline{\overline{S}}_{Aper}$ represents the modal reflection matrix of the open-ended radial cavity. In Fig. 4, $\overline{A}_0$, and $\overline{B}_0$ are vectors containing the complex coefficients of the forward modes and the backward modes at any horizontal plane along the coaxial line, respectively. Similarly, $\overline{A}_1$, and $\overline{B}_1$ are vectors containing the complex coefficients of the forward modes and the backward modes at the input plane of the metasurface (at $Y_1(\rho)$), respectively. Also, the vectors $\overline{A}_2$, and $\overline{B}_2$ contain the complex coefficients of the forward modes and the backward modes at the output plane of the metasurface (at $Y_N(\rho)$), respectively. The modal coefficients in each vector are arranged from the lowest to the highest considered mode. According to the size of the modal vectors ($\overline{A}$, and $\overline{B}$), the modal matrices $\overline{\overline{S}}_{feed}$, $\overline{\overline{S}}_{MTS}$, and $\overline{\overline{S}}_{Aper}$ can be partitioned as

follows (see Fig. 4),

$$\begin{bmatrix}\overline{B}_0\\ \overline{A}_1\end{bmatrix}=\begin{bmatrix}S^{(1,1)}_{feed} & S^{(1,2)}_{feed}\\ S^{(2,1)}_{feed} & S^{(2,2)}_{feed}\end{bmatrix}\begin{bmatrix}\overline{A}_0\\ \overline{B}_1\end{bmatrix} \tag{13}$$

$$\begin{bmatrix}\overline{B}_1\\ \overline{A}_2\end{bmatrix}=\begin{bmatrix}S^{(1,1)}_{MTS} & S^{(1,2)}_{MTS}\\ S^{(2,1)}_{MTS} & S^{(2,2)}_{MTS}\end{bmatrix}\begin{bmatrix}\overline{A}_1\\ \overline{B}_2\end{bmatrix} \tag{14}$$

$$\overline{B}_2 = D_e\overline{\overline{S}}_{Aper}D_e\overline{A}_2, \tag{15}$$

where D_e is an embedding matrix. In (15), embedding is needed since the modal vectors $\overline{A}_2$ and $\overline{B}_2$ are defined at the metasurface output plane, which in general may not be the same as the antenna aperture plane. Since only one mode is considered in the coaxial line, the size of the matrix $\overline{\overline{S}}_{feed}$ is $(N+1)\times(N+1)$, where N is the number of accessible modes in the waveguide. Additionally, the size of the matrix $\overline{\overline{S}}_{MTS}$ is $(2N\times 2N)$. Finally, the size of the reflection matrix $\overline{\overline{S}}_{Aper}$ is $(N\times N)$.

To proceed, (13), and (15) are substituted into (14) to obtain,

$$\begin{bmatrix}\overline{B}_1\\ \overline{A}_2\end{bmatrix}=(L)^{-1}\begin{bmatrix}S^{(1,1)}_{MTS}S^{(2,1)}_{feed}\overline{A}_0\\ S^{(2,1)}_{MTS}S^{(2,1)}_{feed}\overline{A}_0\end{bmatrix}, \tag{16}$$

where L is written as follows,

$$L=\begin{bmatrix}I-S^{(1,1)}_{MTS}S^{(2,2)}_{feed} & -S^{(1,2)}_{MTS}D_eS_{Aper}D_e\\ -S^{(2,1)}_{MTS}S^{(2,2)}_{feed} & I-S^{(2,2)}_{MTS}D_eS_{Aper}D_e\end{bmatrix}, \tag{17}$$

and I is the $N\times N$ identity matrix. From (16), the forward modal vector, $\overline{A}_2$, at the metasurface output plane can be found for a given coaxial excitation $\overline{A}_0$. Once $\overline{A}_2$ is known using (16), the Fourier-Bessel coefficients of the aperture electric field e_n can be easily found using (11). So, we have,

$$\overline{E}=g\left(I+\overline{\overline{S}}_{Aper}\right)D_e\overline{A}_2, \tag{18}$$

where, $\overline{E}$ is defined as in (11), g is defined by (12), and the modal vector $\overline{A}_2$ has been de-embedded to the aperture plane using D_e. The aperture fields can now be obtained from e_n using (8).

To summarize, in order to find the radiated fields from the antenna shown in Fig. 4, due to a given coaxial excitation $\overline{A}_0$, we calculate the modal vector at the metasurface output plane $\overline{A}_2$ using (16). Then, the Fourier-Bessel coefficients of the aperture electric field e_n can be calculated using (18). Finally, from the Fourier-Bessel coefficients of the aperture electric field, we can obtain the aperture field profile using (8).

The Fourier-Bessel coefficients of the aperture electric field e_n uniquely determine the aperture fields. Thus, the optimization objective function (the function to be minimized) F can be straightforwardly written as follows,

$$F=\left\|\overline{E}_{calc}-\overline{E}_{des}\right\|. \tag{19}$$

In each iteration of the optimization $\overline{E}_{calc}$ is calculated using (18). $\overline{E}_{des}$ is a vector containing the Fourier-Bessel coefficient of the desired aperture electric field $\mathrm{E}_{des}(\rho)$. The

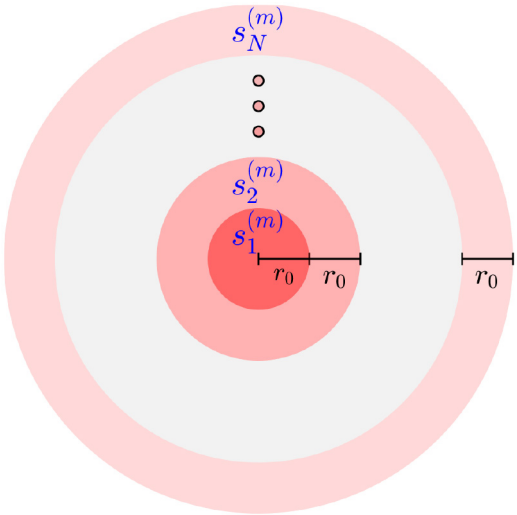

FIGURE 5. The discretization of the electric sheets comprising the metasurface. Each electric sheet is segmented into concentric capacitive annuli with equal width r_0. The annulus width is equal to the ratio of the electric sheet radius R to the number of annuli N. A surface susceptance value $s_n^{(m)}$ is assigned to the *nth* annulus in the *mth* electric sheet.

nth Fourier-Bessel coefficient of the desired aperture electric field e_n^{des} is calculated as follows,

$$e_n^{des}=\frac{\int_0^R \mathrm{E}_{des}(\rho)J_1\left(\frac{j_n}{R}\rho\right)\rho d\rho}{u_n}, \tag{20}$$

where, R, j_n, and u_n are defined as in (1) and (5). Note that, the desired aperture profile $\mathrm{E}_{des}(\rho)$ should be normalized such that the total radiated power equals the total incident power. Doing so ensures that the coaxial line is matched to the radial cavity.

In the optimization routine, each of the constitutive electric sheets of the mode-converting metasurface is assumed to be lossless, and passive. Therefore, the admittance profile of each sheet $Y_m(\rho)$ (see Fig. 3, and Fig. 4) has only an imaginary part,

$$Y_m(\rho)=ib_m(\rho), \tag{21}$$

where $b_m(\rho)$ is a real-valued function and m identifies the sheet number. Furthermore, each sheet is uniformly segmented into N concentric capacitive annuli, as shown in Fig. 5. So, $b_m(\rho)$ is a piece-wise function that can be defined as follows,

$$b_m(\rho)=\begin{cases}s_1^{(m)} & 0<\rho<r_n\\ s_2^{(m)} & r_n<\rho<2r_n\\ \vdots & \\ s_N^{(m)} & (N-1)r_n<\rho<Nr_n,\end{cases} \tag{22}$$

where, $s_1^{(m)}$ through $s_N^{(m)}$ are all positive numbers, $r_n=\frac{R}{N}$, R is the waveguide radius, and N is the total number of capacitive annuli. This particular profile of the electric sheets was chosen since it can be practically realized, as has been demonstrated in [3]. The concentric, capacitive annuli can

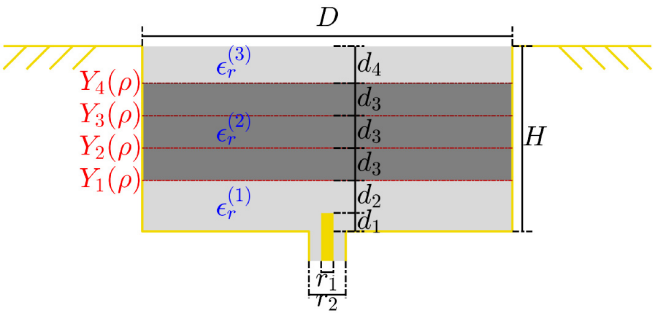

FIGURE 6. Geometrical and materials parameters of the radial Gaussian beam antenna. The mode-converting metasurface used to synthesize the radial Gaussian beam antenna comprises four equally-spaced electric sheets. These electric sheets are labeled $Y_1(\rho)$, $Y_2(\rho)$, $Y_3(\rho)$ and $Y_4(\rho)$.

be realized using a printed metallic cladding on the top and bottom of a thin dielectric substrate. In the following section, an example that illustrates the design procedure is presented. Using the design procedure, an antenna supporting a radially polarized Gaussian beam is synthesized.

IV. RADIAL GAUSSIAN BEAM ANTENNA

In this section, we apply the aperture synthesis method presented in this work to the design of a radial Gaussian beam antenna. A radial Gaussian beam is an example of a cylindrical vector beam. Cylindrical vector beams are solutions to the azimuthal or radial paraxial wave equations [18]. These beams approximately maintain their transverse profile over a considerable distance within the Fresnel zone. For Bessel beams, this distance is known as the non-diffractive range [22], and for Gaussian beams it is known as the Rayleigh length [36]. Because of their diffraction-resisting properties, cylindrical vector beams are ideally suited for wireless links or transfer power within the Fresnel zone [17], [27].

A radial Bessel beam, another type of the cylindrical vector beam, can be generated using a single homogeneous (non-spatially varying) capacitive electric sheet above an over-moded radial cavity [23]. This is possible since a Bessel beam is an eigenmode of a homogeneous radial cavity. However, this is not generally the case for other cylindrical vector beams, including the radial Gaussian beam [37]. As we will see, generating a radial Gaussian beam requires the excitation of multiple TM_{0n} modes with different modal coefficients. Therefore, multiple inhomogeneous electric sheets will be needed to generate a radial Gaussian beam. In this section, a radial Gaussian beam antenna will be designed using idealized impedance sheets by following the procedure outlined in Section III. A practical realization of the proposed antenna will be the topic of a future publication. The ideal sheet design can be practically realized using patterned claddings, as shown in [3].

In this example, the radial Gaussian beam antenna is designed to have a uniform phase profile at 10 GHz. The metasurface, as shown in Fig. 6, consists of four cascaded electric sheets that are equally spaced. Each of these four sheets is uniformly segmented into 15 capacitive annuli (see Fig. 5). The dimensions of the antenna are shown in Table 1 in accordance with Fig. 6. The dielectric constants of the spacers shown in Fig. 6 are $\epsilon_r^{(1)} = \epsilon_r^{(3)} = 1.07$, and $\epsilon_r^{(2)} = 3$. Commercial availability was factored into the choice of the material parameters and the dimensions of the antenna. Also, the coaxial line was chosen such that it has a 50 ohm input impedance. The aperture profile of a uniform-phase, radial Gaussian beam antenna takes the following form [17],

TABLE 1. Dimensions of the radial Gaussian beam antenna (*mm*).

D	H	r_1	r_2	d_1	d_2	d_3	d_4
150	17.27	1.27	2.9	3.43	2.92	1.52	6.35

$$\mathrm{E}_g(\rho) = \sqrt{2\frac{\rho^2}{w^2}}e^{\frac{\rho^2}{w^2}}, \tag{23}$$

where, w is the beam waist. To ensure minimal edge diffraction, the beam waist w should be chosen to be at most half the aperture radius. As given in Table 1, the aperture diameter is $D = 5\lambda$ at 10 GHz (the design frequency). Thus, the waist is $w = 1.25\lambda$ at 10 GHz. Based on the size and the material parameters of the cavity and metasurface, a total of 20 TM_{0n} modes are considered in the interaction between the coaxial feed, the metasurface, and the cavity. In the cavity, 5 of these 20 TM_{0n} modes are propagating. However, due to the tight spacing between the metasurface sheets, a total of 80 TM_{0n} modes are considered in the interaction between the individual sheets of the metasurface. Outside the metasurface, only 20 modes of these 80 modes are considered in the cavity and the other 60 modes are terminated in their reactive wave impedances, as explained in [3]. The magnitude and phase of the 20 modes considered in the modal distribution of the desired Gaussian beam are shown in Fig. 7a. They are found by substituting (23) into (20). The spatial profile of the desired Gaussian beam, as well as the desired profile constructed with 20 modes, are shown in Fig. 7b. Clearly, 20 modes are sufficient to capture the details of the desired Gaussian beam.

To proceed, we substitute the modal distribution of the desired Gaussian beam, shown in Fig. 7a, into the objective function (19). Following the design procedure outlined in Section III, the susceptances of the annuli are optimized to minimize the objective function (19). The optimization was performed using the *interior-point* algorithm within the built-in MATLAB function *fmincon*. The optimal susceptance annuli are shown in Fig. 8. The metasurface electric sheets are lossless, as stated in (21). Hence only the susceptance is shown in Fig. 8. The performance of the designed antenna was verified using the 3D full wave solver ANSYS HFSS. Lossless conditions were assumed in the simulation. The aperture profile obtained from ANSYS HFSS is nearly identical to the desired Gaussian beam aperture, as shown in Fig. 9a. The radiation pattern of the antenna, shown in Fig. 9b, and Fig. 9c, has a Gaussian shape with very low

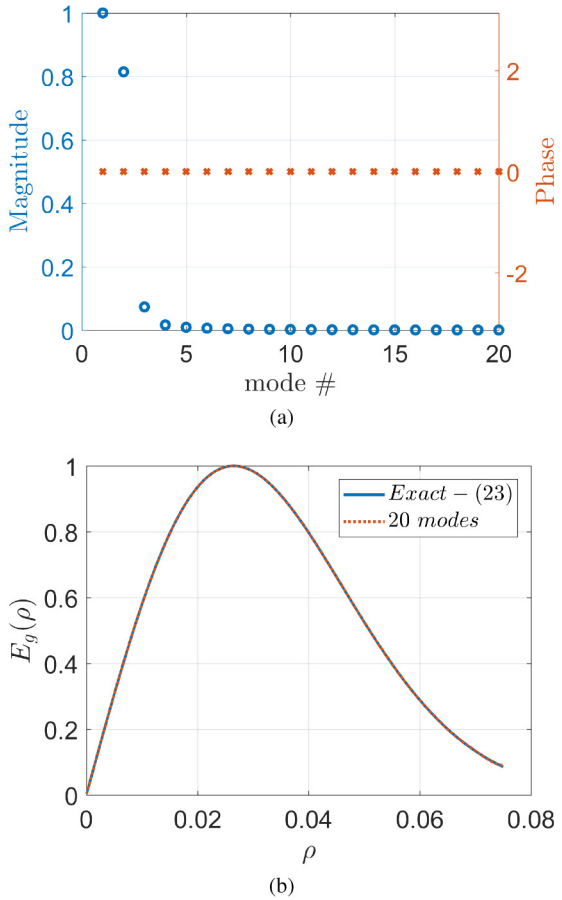

FIGURE 7. Modal and spatial profiles of the desired Gaussian beam aperture. (a) Modal distribution of the desired Gaussian beam aperture with 20 modes considered. (b) Exact and approximate spatial profiles of the desired Gaussian beam aperture. The exact profile is evaluated using (23), and approximate profile is evaluated using the modal distribution in (a).

side lobes. This further confirms the aperture's Gaussian profile. The reflection coefficient at 10 GHz, calculated from ANSYS HFSS, is approximately -22 dB. The matching was achieved by ensuring that the total radiated power equals the total input power. The directivity of the antenna calculated using ANSYS HFSS was 16 dB.

The proposed radial Gaussian beam metasurface antenna has a height and weight advantage over typical Gaussian horn antennas. As given in Table 1, the total height of the antenna is almost equal to $H = .55\lambda$ at the design frequency. This height is substantially lower than that of Gaussian horn antennas with same aperture size. It is also lower than that of other planar Gaussian beam antennas reported in literature. A Gaussian beam antenna array is reported in [38], which consists of an array of 16×16 elements that are fed using a lossy corporate feed. This is in contrast to the proposed antenna where the feed is a simple lossless coaxial probe placed at the center of a radial cavity. A planar antenna has also been reported in [39] that generates a linearly polarized Gaussian beam. The antenna uses planar and spherical mirrors to transform a guided-mode to a resonator mode that has a Gaussian shape.

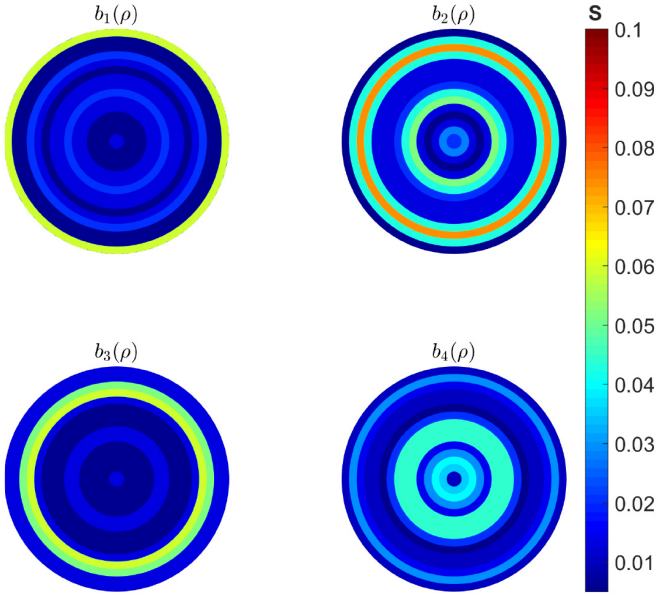

FIGURE 8. The optimized susceptance profiles of the sheets comprising the cascaded-sheet metasurface used in the radial Gaussian beam antenna.

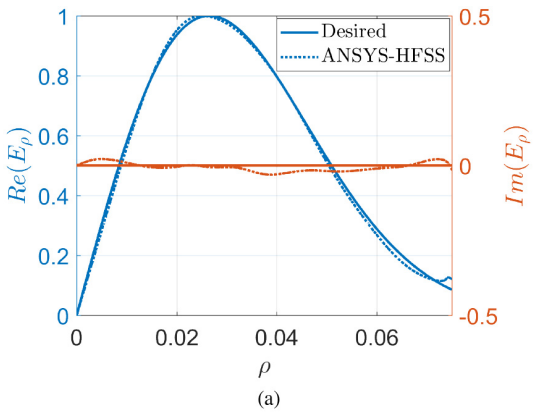

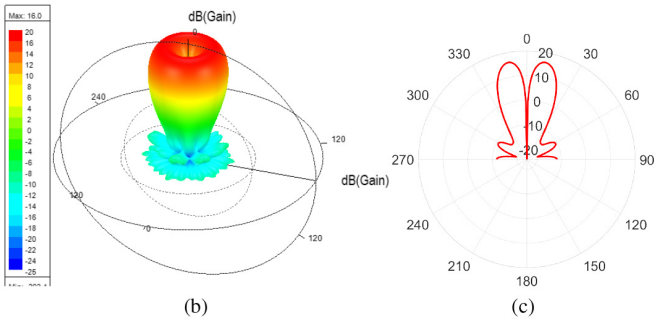

FIGURE 9. Simulated performance of the designed radial Gaussian beam antenna using the commercial full wave solver ANSYS HFSS. (a) The real and the imaginary parts of the antenna aperture profile. The desired Gaussian profile is shown as well. (b) The far field radiation pattern of the radial Gaussian beam antenna. (c) The far field radiation pattern of the radial Gaussian beam antenna as a function of θ evaluated at the plane $x = 0$.

V. CONCLUSION

A general method to synthesize azimuthally-invariant, TM apertures using low-profile, simple-to-feed, cascaded-sheet metasurface antennas was proposed in this paper. The

proposed antennas consist of a coaxially-excited radial cavity topped by a mode-converting metasurface. The mode-converting metasurafce is the mainstay of the proposed antenna. It plays two fundamental roles. First, it establishes the desired aperture profile by converting the modal distribution of the excitation to the modal distribution of the desired aperture. Second, it impedance matches the coaxial feed to the cavity. Unlike most metasurface antennas, the proposed antenna can be designed to meet specific near field and far field criteria. Additionally, the cascaded-sheet model of the metasurface is more straightforward to realize than an idealized bianisotropic sheet model.

Structurally, the antenna can be divided into three main building blocks: the coaxial-to-waveguide junction, the open-ended radial cavity, and the mode-converting metasurface. Using modal network theory, each building block of the antenna is described by a modal scattering matrix. Cascading the modal scattering matrices of the building blocks through simple matrix operations allows the overall antenna to be analyzed. An optimization-based design procedure was developed to synthesize the proposed metasurface antennas. The admittance profiles of the constitutive electric sheets of the mode-converting metasurface are optimized to establish the desired aperture profile and to impedance match the coax feed to the radial cavity. To illustrate the design procedure, a radial Gaussian beam antenna was synthesized at 10 GHz. The antenna has a diameter of 5λ at the design frequency. The performance of the antenna was verified using a commercial full wave electromagnetic solver. The antenna has a subwavelength height. Thus, it has a height advantage over typical Gaussian horn antennas with similar aperture sizes.

Although the discussion in the paper was focused on TM, azimuthally-invariant apertures, the presented design procedure can be generalized to include TE fields as well as azimuthal variation. Future work will include adding multiple coaxial feeds and additional sheets to realize low-profile MIMO metasurface antennas.

APPENDIX
MODAL REFLECTION MATRIX OF AN OPEN-ENDED RADIAL CAVITY

The modal reflection matrix $\overline{\overline{S}}_{Aper}$ of an open-ended waveguide relates the reflected modes to the incident modes at the waveguide aperture. Given that a sufficient number of modes are considered, the modal reflection matrix S_{Aper} completely determines the aperture fields for any arbitrary set of incident modes. Recall from Section II, the electric field expansion on the waveguide side and on the free space side, respectively,

$$E_\rho^{z=0^-} = \sum_{n=1}^{N} \frac{\sqrt{\eta_n}}{u_n}(a_n + b_n)\ J_1\left(\frac{j_n}{R}\rho\right) \tag{24}$$

$$E_\rho^{z=0^+} = \sum_{n=1}^{N} \frac{e_n}{u_n}\ J_1\left(\frac{j_n}{R}\rho\right), \tag{25}$$

where, a_n and b_n denote the forward and backward modal coefficients within the waveguide, and e_n are the electric field coefficients of the aperture. The parameters, j_n, R, η_n, k_{zn}, and u_n are defined as in (1), (3), (4), and (5). Note that the superscript $z = 0^-$ indicates that we are approaching the aperture from below, or from the waveguide side. Likewise, the superscript $z = 0^+$ indicates that we are approaching the aperture from above, or from the free space side. Also, recall the magnetic field expansion on the waveguide side and on the free space side are,

$$H_\phi^{z=0^-} = \sum_{n=1}^{N} \frac{1}{u_n\sqrt{\eta_n}}(a_n - b_n)\ J_1\left(\frac{j_n}{R}\rho\right) \tag{26}$$

$$H_\phi^{z=0^+} = \sum_{n=1}^{N} \frac{h_n}{u_n}\ J_1\left(\frac{j_n}{R}\rho\right), \tag{27}$$

where, h_n are the magnetic field coefficients of the aperture.

The modal reflection matrix $\overline{\overline{S}}_{Aper}$ will be written in terms of the spectral admittance matrix $\overline{\overline{B}}$. The spectral admittance matrix $\overline{\overline{B}}$ relates the electric field coefficients of the aperture e_n to the magnetic field coefficients of the aperture h_n via the spectral Green's functions. Using the spectral Green's function, we can write the tangential magnetic field at the aperture in terms of the tangential electric field at the aperture, for the case of azimuthal symmetry, as follows [17],

$$H_\phi(\rho) = \frac{k_0}{\eta_0}\int_0^\infty \frac{k_\rho}{k_z} J_1(k_\rho\rho)\int_0^R E_\rho(\rho')J_1(k_\rho\rho')\rho' d\rho' dk_\rho, \tag{28}$$

where, k_0 is the free space wavenumber, η_0 is the free space characteristic impedance, and $k_z = \sqrt{k_0^2 - k_\rho^2}$. Substituting (25) and (27) into (28), and exploiting the orthogonality relations of Bessel functions [3], one can obtain the following relations

$$\overline{H} = \overline{\overline{B}}\ \overline{E} \tag{29}$$

$$\overline{\overline{B}}(m,n) = \frac{k_0}{\eta_0}\int_0^\infty \frac{k_\rho}{k_z} L\left(\frac{j_n}{R}, k_\rho\right) L\left(\frac{j_m}{R}, k_\rho\right) dk_\rho \tag{30}$$

$$L\left(\frac{j_q}{R}, k_\rho\right) = \frac{\int_0^R J_1\left(\frac{j_q}{R}\rho\right) J_1(k_\rho\rho)\rho d\rho}{u_q}, \tag{31}$$

where, $\overline{E} = [e_1, e_2 \ldots, e_N]^T$, and $\overline{H}$ is defined similarly. The integral in (31) is known in closed form and is reported in [40].

The following two equations can be obtained by enforcing field continuity. In other words, we set (24) equal to (25), and (26) equal to (27). So, we can write,

$$g\left[\overline{A} + \overline{B}\right] = \overline{E}, \tag{32}$$

$$(g)^{-1}\left[\overline{A} - \overline{B}\right] = \overline{\overline{B}}\ \overline{E}, \tag{33}$$

where, $\overline{A} = [a_1, a_2 \ldots, a_N]^T$, $\overline{B} = [b_1, b_2 \ldots, b_N]^T$, and g is a diagonal matrix defined as in (12). It should be noted that (29) was used in (33). Solving (32), and (33) for $\overline{B}$, we have the following,

$$\overline{B} = \left((g)^{-1} - g\overline{\overline{B}}\right)\left((g)^{-1} + g\overline{\overline{B}}\right)^{-1}\overline{A}. \tag{34}$$

Comparing (34) to (10), we see that we have obtained the modal reflection matrix $\overline{\overline{S}}_{Aper}$.

REFERENCES

[1] H.-H. Hsiao, C. H. Chu, and D. P. Tsai, "Fundamentals and applications of metasurfaces," *Small Methods*, vol. 1, no. 4, 2017, Art. no. 1600064.

[2] C. L. Holloway, E. F. Kuester, J. A. Gordon, J. O'Hara, J. Booth, and D. R. Smith, "An overview of the theory and applications of metasurfaces: The two-dimensional equivalents of metamaterials," *IEEE Antennas Propag. Mag.*, vol. 54, no. 2, pp. 10–35, Apr. 2012.

[3] F. Alsolamy and A. Grbic, "Modal network formulation for the analysis and design of mode-converting metasurfaces in cylindrical waveguides," *IEEE Trans. Antennas Propag.*, early access, Jan. 8, 2021, doi: 10.1109/TAP.2020.3048590.

[4] A. Epstein and G. V. Eleftheriades, "Arbitrary power-conserving field transformations with passive lossless omega-type bianisotropic metasurfaces," *IEEE Trans. Antennas Propag.*, vol. 64, no. 9, pp. 3880–3895, Sep. 2016.

[5] A. Ranjbar and A. Grbic, "Analysis and synthesis of cascaded metasurfaces using wave matrices," *Phys. Rev. B*, vol. 95, May 2017, Art. no. 205114.

[6] C. Pfeiffer and A. Grbic, "Bianisotropic metasurfaces for optimal polarization control: Analysis and synthesis," *Phys. Rev. Appl.*, vol. 2, Oct. 2014, Art. no. 044011.

[7] C. L. Holloway, E. F. Kuester, and A. Dienstfrey, "Characterizing metasurfaces/metafilms: The connection between surface susceptibilities and effective material properties," *IEEE Antennas Wireless Propag. Lett.*, vol. 10, pp. 1507–1511, 2011.

[8] D. Zaluški, A. Grbic, and S. Hrabar, "Analytical and experimental characterization of metasurfaces with normal polarizability," *Phys. Rev. B*, vol. 93, no. 15, 2016, Art. no. 155156.

[9] M. Faenzi *et al.*, "Metasurface antennas: New models, applications and realizations," *Sci. Rep.*, vol. 9, no. 1, pp. 1–14, 2019.

[10] Z. Li *et al.*, "Controlling propagation and coupling of waveguide modes using phase-gradient metasurfaces," *Nat. Nanotechnol.*, vol. 12, no. 7, pp. 675–683, 2017.

[11] B. O. Raeker and A. Grbic, "Compound metaoptics for amplitude and phase control of wave fronts," *Phys. Rev. Lett.*, vol. 122, no. 11, 2019, Art. no. 113901.

[12] V. G. Ataloglou and G. V. Eleftheriades, "Surface-waves optimization for beamforming with a single omega-bianisotropic huygens' metasurface," in *Proc. IEEE Int. Symp. Antennas Propag. North Amer. Radio Sci. Meeting*, Montreal, QC, Canada, 2020, pp. 905–906.

[13] B. H. Fong, J. S. Colburn, J. J. Ottusch, J. L. Visher, and D. F. Sievenpiper, "Scalar and tensor holographic artificial impedance surfaces," *IEEE Trans. Antennas Propag.*, vol. 58, no. 10, pp. 3212–3221, Oct. 2010.

[14] G. Minatti *et al.*, "Modulated metasurface antennas for space: Synthesis, analysis and realizations," *IEEE Trans. Antennas Propag.*, vol. 63, no. 4, pp. 1288–1300, Apr. 2015.

[15] M. Bodehou, C. Craeye, E. Martini, and I. Huynen, "A quasi-direct method for the surface impedance design of modulated metasurface antennas," *IEEE Trans. Antennas Propag.*, vol. 67, no. 1, pp. 24–36, Jan. 2019.

[16] J. Budhu and A. Grbic, "Perfectly reflecting metasurface reflectarrays: Mutual coupling modeling between unique elements through homogenization," *IEEE Trans. Antennas Propag.*, vol. 69, no. 1, pp. 122–134, Jan. 2021.

[17] F. Alsolamy, W. A. Alomar, and A. Grbic, "Cylindrical vector beams for wireless power transfer," *IEEE Trans. Antennas Propag.*, vol. 69, no. 3, pp. 1716–1727, Mar. 2021.

[18] Q. Zhan, "Cylindrical vector beams: From mathematical concepts to applications," *Adv. Opt. Photon.*, vol. 1, no. 1, pp. 1–57, 2009.

[19] R. Sorrentino and F. Alimenti, "Waveguide discontinuities," in *Encyclopedia of RF and Microwave Engineering*. New Jersey, NJ, USA: Amer. Cancer Soc., 2005.

[20] R. F. Harrington, "Microwave networks," in *Time-Harmonic Electromagnetic Fields*. New York, NY, USA: IEEE, 2001, pp. 381–446.

[21] D. M. Pozar, "Microwave network analysis," in *Microwave Engineering*, 4th ed. Hoboken, NJ, USA: Wiley, 2011, pp. 165–222.

[22] M. Ettorre and A. Grbic, "Generation of propagating bessel beams using leaky-wave modes," *IEEE Trans. Antennas Propag.*, vol. 60, no. 8, pp. 3605–3613, Aug. 2012.

[23] M. Ettorre, S. M. Rudolph, and A. Grbic, "Generation of propagating bessel beams using leaky-wave modes: Experimental validation," *IEEE Trans. Antennas Propag.*, vol. 60, no. 6, pp. 2645–2653, Jun. 2012.

[24] W. Fuscaldo, G. Valerio, A. Galli, R. Sauleau, A. Grbic, and M. Ettorre, "Higher-order leaky-mode bessel-beam launcher," *IEEE Trans. Antennas Propag.*, vol. 64, no. 3, pp. 904–913, Mar. 2016.

[25] C. Pfeiffer and A. Grbic, "Controlling vector bessel beams with metasurfaces," *Phys. Rev. Appl.*, vol. 2, Oct. 2014, Art. no. 044012.

[26] F. E. Gardiol, "Open-ended waveguides: Principles and applications," in *Advances in Electronics and Electron Physics*, vol. 63, P. W. Hawkes, Ed. New York, NY, USA: Academic, 1985, pp. 172–174.

[27] J. D. Heebl, M. Ettorre, and A. Grbic, "Wireless links in the radiative near field via bessel beams," *Phys. Rev. Appl.*, vol. 6, Sep. 2016, Art. no. 034018.

[28] F. Alsolamy and A. Grbic, "A metasurface based mode converter," in *Proc. 13th Int. Congr. Artif. Mater. Novel Wave Phenom. (Metamaterials)*, Rome, Italy, 2019, pp. 29–31.

[29] F. Alsolamy and A. Grbic, "Mode conversion in cylindrical waveguides using metasurfaces," in *Proc. 14th Int. Congr. Artif. Mater. Novel Wave Phenom. (Metamaterials)*, New York, NY, USA, 2020, pp. 75–77.

[30] F. Alsolamy and A. Grbic, "Cylindrical aperture synthesis with metasurfaces," in *Proc. 14th Eur. Conf. Antennas Propag. (EuCAP)*, Copenhagen, Denmark, 2020, pp. 1–2.

[31] H. F. Johnson, "An improved method for computing a discrete Hankel transform," *Comput. Phys. Commun.*, vol. 43, no. 2, pp. 181–202, 1987.

[32] N. Baddour and U. Chouinard, "Theory and operational rules for the discrete Hankel transform," *J. Opt. Soc. Amer. A*, vol. 32, no. 4, pp. 611–622, 2015.

[33] J. W. Tao and H. Baudrand, "Multimodel variational analysis of uniaxial waveguide discontinuities," *IEEE Trans. Microw. Theory Techn.*, vol. 39, no. 3, pp. 506–516, Mar. 1991.

[34] A. Wexler, "Solution of waveguide discontinuities by modal analysis," *IEEE Trans. Microw. Theory Techn.*, vol. 15, no. 9, pp. 508–517, Sep. 1967.

[35] G. V. Eleftheriades, A. S. Omar, L. P. B. Katehi, and G. M. Rebeiz, "Some important properties of waveguide junction generalized scattering matrices in the context of the mode matching technique," *IEEE Trans. Microw. Theory Techn.*, vol. 42, no. 10, pp. 1896–1903, Oct. 1994.

[36] D. McGloin and K. Dholakia, "Bessel beams: Diffraction in a new light," *Contemp. Phys.*, vol. 46, no. 1, pp. 15–28, 2005.

[37] F. Alsolamy and A. Grbic, "Radial Gaussian beam metasurface antenna," in *Proc. IEEE Int. Symp. Antennas Propag. North Amer. Radio Sci. Meeting*, Montreal, QC, Canada, 2020, pp. 743–744.

[38] C. Pfeiffer, T. Steffen, and G. Kakas, "Uniform beamwidth UWB feed antenna using lossy transmission lines," *Progr. Electromagn. Res.*, vol. 165, pp. 119–130, Oct. 2019.

[39] T. Matsui, M. Kiyokawa, and N. Hirose, "Millimeter-wave Gaussian-beam antenna and integration with planar circuits," in *IEEE MTT-S Int. Microw. Symp. Dig.*, vol. 1. San Francisco, CA, USA, 1996, pp. 393–396.

[40] F. Bowman, "Lommel's integrals," in *Introduction to Bessel Functions*. New York, NY, USA: Dover, 1958, p. 101.

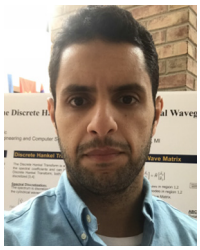

FARIS ALSOLAMY (Member, IEEE) received the B.Sc. degree in electrical and computer engineering from King Abdulaziz University, Saudi Arabia, in 2012. He currently pursuing the Graduate degree with the University of Michigan. From February 2013 to August 2015, he worked as an Antenna Engineer with the King Abdulaziz City of Science and Technology (KACST). During that period, he has spent most of his time in South Africa, to work on collaborative project between KACST and CSIR. His tasks included the design of a wide scanning angle antenna for radar applications.

ANTHONY GRBIC (Fellow, IEEE) received the B.A.Sc., M.A.Sc., and Ph.D. degrees in electrical engineering from the University of Toronto, Canada, in 1998, 2000, and 2005, respectively.

In 2006, he joined the Department of Electrical Engineering and Computer Science, University of Michigan, Ann Arbor, MI, USA, where he is currently a Professor. His research interests include engineered electromagnetic structures (metamaterials, metasurfaces, electromagnetic band-gap materials, frequency-selective surfaces), antennas, microwave circuits, and analytical electromagnetics/optics. He was a recipient of the AFOSR Young Investigator Award as well as the NSF Faculty Early Career Development Award in 2008, the Presidential Early Career Award for Scientists and Engineers in January 2010. He also received the Outstanding Young Engineer Award from the IEEE Microwave Theory and Techniques Society, the Henry Russel Award from the University of Michigan, the Booker Fellowship from the United States National Committee of the International Union of Radio Science in 2011, and the University of Michigan Faculty Recognition Award for outstanding achievement in scholarly research, excellence as a teacher, an advisor and a mentor, and distinguished service to the institution and profession in 2018. He was an inaugural recipient of the Ernest and Bettine Kuh Distinguished Faculty Scholar Award in the Department of Electrical and Computer Science, University of Michigan in 2012. He served as a Technical Program Co-Chair in 2012, and a Topic Co-Chair in 2016 and 2017 for the IEEE International Symposium on Antennas and Propagation and USNC-URSI National Radio Science Meeting. He was an Associate Editor for IEEE ANTENNAS AND WIRELESS PROPAGATION LETTERS from 2010 to 2015. He will be a Distinguished Microwave Lecturer for the IEEE Microwave Theory and Techniques Society starting January 2022.